Available online at www.sciencedirect.com

ScienceDirect

Energy Procedia 4 (2011) 4457–4464

Energy Procedia

www.elsevier.com/locate/procedia

GHGT-10

Managing Chemistry Underground: Is Co-Sequestration an Option in Selected Formations?

Diana H. Bacon[a] * and Ellyn M. Murphy[a]

[a]*Pacific Northwest National Laboratory, Richland, Washington USA*

Abstract

Geochemical simulations indicate that co-injection of CO_2 and SO_2 results in mineral sequestration of SO_2. The amounts sequestered are greater and more persistent in dolomite and basalt than in glauconitic sandstone. In a predominantly dolomite formation, dissolution of calcite, and to a lesser extent, dolomite, will provide Ca in solution to promote the precipitation of anhydrite, thus removing the SO_2 from solution. In basalt, dissolution of basaltic glass under acidic conditions provides Ca and Fe in solution, which promotes the sequestration of SO_2 as anhydrite and, eventually, pyrite. As magnetite in the formation is consumed, pyrite redissolves. In the basalt, 86% to 47% of the SO_2 remains sequestered after 5000 years. In glauconitic sandstone, SO_2 precipitates as alunite, but it eventually redissolves. After 5000 years, 87% to 0% of the SO_2 remains sequestered in the glauconitic sandstone. In all cases, co-injection of 1% SO_2 with CO_2 did not appreciably reduce the amount of CO_2 sequestered, and did not induce a measureable change in porosity versus injection of CO_2 alone.

Keywords: co-sequestration, carbon dioxide, sulfur dioxide, geochemical reaction modeling.

Introduction

Electricity generation from coal, estimated to be 41% globally, will continue to play a critical role for decades as the world transitions to renewable energy and energy technologies that do not emit greenhouse gases. For the two largest economies and users of electricity, the U.S. and China, coal is abundant, affordable and engrained within the existing infrastructure. Coal power plants currently emit approximately 36% of US and over 75% of China CO_2 emissions. New power plant designs and technologies offer promise, but any meaningful reductions in greenhouse gas emissions will necessitate addressing existing coal-based power plants, which may be operational for decades.

Developing countries have a greater reliance on coal-based electricity, yet understandably have been hesitant to install or use costly unit processes that sequentially remove key pollutants from the flue gas. These countries, although not insensitive to climate change, are more urgently concerned with the impact of emissions on human

* Corresponding author. Tel.: +1-509-372-6132; fax: +1-509-372-6089.
E-mail address: diana.bacon@pnl.gov.

doi:10.1016/j.egypro.2011.02.400

health and environmental quality. Additionally, the decision to retrofit a coal-based power plant for carbon capture and geologic sequestration will be driven by cost. These cost estimates typically take into account the output and age of the plant, available space for the capture facility (up to 30% additional space), and proximity to a geologic sequestration site. In order to address these issues that drive the retrofit cost, new, integrated processes for capture and co-sequestration must be considered. Innovative ideas, such as using the mineralogy of deep saline systems to co-sequester NO_x, SO_x, and CO_2, or just SO_x and CO_2, could significantly lower retrofit costs. This approach would also allow developing countries to address their health and environmental quality concerns, while also addressing carbon dioxide emissions.

One of the key factors to be considered in geologic co-sequestration of NO_x, SO_x and CO_2 is the effect that these dissolved supercritical fluids will have on the pH of the formation water, and hence on the porosity of the formation. The porosity of the formation may increase through dissolution of formation minerals or decrease via secondary mineral precipitation, thus affecting the sequestration capacity of the formation. Which of these scenarios occurs depends on a complex array of factors including formation and caprock mineralogy, pore-water chemistry, and the composition of the injectate.

In order to determine the geologic scenarios where co-sequestration is practical, we present a modeling survey with a variety of model parameters. Model parameters include flue gas composition, salinity, formation mineralogy, and formation depth and temperature. Formation types include sandstone, dolomite, and basalt.

Methods

Numerical simulation of CO_2 injection into deep geologic reservoirs requires modeling complex, coupled hydrologic, chemical, and thermal processes, including multi-fluid flow and transport, partitioning of CO_2 into the aqueous phase, and chemical interactions with aqueous fluids and rock minerals. The simulations conducted for this investigation were executed with the STOMP-CO2-R (water, CO_2, salt, energy and reactions) simulator [1]. STOMP has been verified against other codes used for simulation of geologic disposal of CO_2 as part of the GeoSeq code comparison study, and has been used in previous investigations of CO_2 injection potential at several sites, including co-sequestration of SO_2 into dolomite and sandstone. Simulations were conducted that considered geochemical reactions involving the minerals present in the formation, the formation brine and injected supercritical fluids. These simulations used the batch geochemistry solution module ECKEChem (Equilibrium-Conservation-Kinetic Equation Chemistry). This add-on module to STOMP is described in an addendum to the STOMP User's Guide [2].

ECKEChem uses an operator splitting reactive transport scheme. The operating splitting scheme solves the reactive species transport separately from the reactive species chemistry equations. The coupled nonisothermal multifluid flow and transport equations are solved sequentially with the reactive transport equations; and the reactive transport equations are solved sequentially as two components: 1) multifluid component and kinetic species transport and 2) batch chemistry. ECKEChem uses a noniterative sequential solution scheme to minimize computational costs. To reduce the number of transported species only mobile component and kinetic species are transported, which requires that transport properties, such as diffusion and dispersion coefficients are species independent. In this mathematical formulation reactive species are either components of the coupled flow and transport equations (e.g., water or CO_2) or dilute solutes; where, the principal assumption associated with dilute solutes is that phase properties are independent of solute concentrations. Reactive species that are components of the flow and transport equations are linked to the components via source/sink terms. For these simulations, the B-dot activity model was used [3].

The model domain was a single node one cubic meter in size. Simulations considered three different depths (Table 1). In order to calculate the ambient pressure and temperature at each depth, a geothermal gradient of 0.025 ºC/m and a hydrostatic gradient of 10,518 Pa/m were assumed. For each of the three depths, two cases were considered, one where 10 kg of supercritical CO_2 was injected over a one year period, and a second where 9.9 kg of CO_2 and 0.1 kg of SO_2 [4] was injected. Three different formations were considered, basalt, dolomite and glauconitic sandstone.

Table 1. Temperature and pressure at three depths.

Depth, m	Pressure, MPa	Temperature, ºC
1000	10.619	40
2000	21.137	65
3000	31.655	90

Basalt

The dissolution of Columbia River Basalt under mildly acidic conditions has been assumed to be controlled by the following rate reaction:

$$r = k_{ref}\ A \exp\left[\frac{-E_a}{R}\left(\frac{1}{T}-\frac{1}{T_{ref}}\right)\right]\left(1-\frac{Q}{K_{eq}}\right)10^{(-\eta\ pH)} \quad (1)$$

where r is the reaction rate in mol s^{-1}, A is the surface area in m^2, k is the intrinsic rate constant in mol m^{-2} s^{-1}, E_a is the activation energy in kJ mol^{-1}, R is the universal gas constant, T is temperature in degrees Kelvin, Q is the ion activity product, K_{eq} is the equilibrium constant, and η is the pH power law coefficient. The mineral composition of the basalt, rate parameters for the primary constituents of the basalt, and secondary minerals that may precipitate after injection of CO_2 (Table 2) are taken from laboratory experiments on Columbia River Basalt [5] and related batch chemistry simulations using EQ3/6 [6]. Kinetic data for secondary minerals were taken from published rates [7, 8]. Mineral densities, pertinent equilibrium aqueous reactions and their equilibrium coefficients at the three temperatures were determined using the EQ3/6 version 8.0 COMP database [6]. Initial conditions for aqueous species concentrations were based on groundwater sampling [9] from test zone 8B. This formation water is the least saline of the three considered in this paper, with a sodium chloride concentration of 4×10^{-3} M. The porosity of the basalt flow tops was estimated to be 10%.

Table 2. Minerals included in basalt simulation.

Mineral	Composition	Density, kg/m^3	Volume, %	Surface Area, cm^2/g	k_{25}, mol/m^2 s	E_a, kJ/mol
Albite-high	$NaAlSi_3O_8$	2610	15.26	23	2.75×10^{-13}	65.0
Anorthite	$CaAl_2(SiO_4)_2$	2760	18.40	23	7.59×10^{-10}	17.8
Diopside	$CaMgSi_2O_6$	3280	12.89	19	7.76×10^{-12}	40.6
Hedenbergite	$CaFe(SiO_3)_2$	3630	4.30	19	7.76×10^{-12}	40.6
Mesostasis	$Si_{0.548}Al_{0.19}Ca_{0.102}Fe_{0.119}K_{0.006}Mg_{0.0826}Mn_{0.0015}Na_{0.0581}Ti_{0.017}O_{1.764}$	2650	38.25	22	7.17×10^{-08} (100ºC)	30.3
Magnetite	Fe_3O_4	5200	0.90	12	1.66×10^{-11}	18.6
Anatase	TiO_2	3900	0	10	6.92×10^{-12}	37.9
Anhydrite	$CaSO_4$	2960	0	10	6.50×10^{-4}	14.3
Beidellite-Ca	$Ca_{0.165}Al_{2.33}Si_{3.67}O_{10}(OH)_2$	2830	0	10	1.66×10^{-13}	35.0
Beidellite-K	$K_{0.33}Al_{2.33}Si_{3.67}O_{10}(OH)_2$	2790	0	10	1.66×10^{-13}	35.0
Beidellite-Mg	$Mg_{0.165}Al_{2.33}Si_{3.67}O_{10}(OH)_2$	2950	0	10	1.66×10^{-13}	35.0
Calcite	$CaCO_3$	2710	0	10	1.50×10^{-6}	23.5
Chalcedony	SiO_2	2650	0	10	5.89×10^{-13}	62.8
Dawsonite	$NaAlCO_3(OH)_2$	2420	0	10	1.00×10^{-7}	40.6
Dolomite	$CaMg(CO_3)_2$	2860	0	10	2.90×10^{-8}	52.2
Pyrite	FeS_2	5010	0	10	2.82×10^{-15}	57.9
Rhodochrosite	$MnCO_3$	3700	0	10	4.57×10^{-10}	23.5
Siderite	$FeCO_3$	3940	0	10	4.57×10^{-10}	23.5

Dolomite

The dolomite formation considered in this paper was based on the Copper Ridge dolomite [10]. ELAN analysis of well logs indicates that the Copper Ridge formation is predominantly composed of dolomite, with secondary amounts of anhydrite, calcite, illite, and quartz. Kinetic data (Table 3) for all minerals were taken from published rates [7]. Mineral densities, pertinent equilibrium aqueous reactions and their equilibrium coefficients at the three temperatures were determined using the EQ3/6 version 8.0 COMP database [6]. Initial conditions for aqueous

species concentrations were based on groundwater sampling from the overlying Rose Run dolomitic sandstone [11]. This formation has the most saline water chemistry of the three formations, with a sodium chloride concentration of 2.4 M. The average porosity was 4%.

Table 3. Minerals considered in dolomite simulation.

Mineral	Composition	Density, kg/m^3	Volume, %	Surface Area, cm^2/g	k_{25}, mol/m^2 s	E_a, kJ/mol
Anhydrite	$CaSO_4$	2960	0.19	10	6.50E-04	14.3
Calcite	$CaCO_3$	2710	0.19	10	1.50E-06	23.5
Dolomite	$CaMg(CO_3)_2$	2860	76.7	10	2.90E-08	52.2
Hematite	Fe_2O_3	5270	0.1	10	2.15E-15	66.2
Quartz	SiO_2	2650	15.4	10	4.60E-14	87.5

Glauconitic Sandstone

The glauconitic sandstone aquifer (Alberta Sedimentary Basin, Canada) is a medium- to fine-grained litharenite. The average mineral composition is shown in Table 4. The average porosity is 12%. A representative glauconite chemical composition and thermodynamic properties were estimated from descriptions of the mineralogical compositions of glauconite and its paragenesis as reported in the published literature [12]. Oligoclase was incorporated as a solid solution of plagioclase, and the thermodynamic properties of oligoclase were calculated from calorimetric studies of plagioclase solid solutions reported in the literature. Mineral densities, pertinent equilibrium aqueous reactions and their equilibrium coefficients at the three temperatures were determined using the EQ3/6 version 8.0 COMP database [6]. Furthermore, organic matter was assumed to be present in the glauconitic sandstone, and was represented by the generic composition, CH_2O. Goethite (FeOOH) was added as a possible secondary mineral phase. The initial water chemistry used in the simulation was a pure 1.0 M solution of sodium chloride at a temperature of 54 ˚C, a pH of 7, and an Eh of -0.1.

Table 4. Minerals included in glauconitic sandstone simulation.

Mineral	Composition	Density, kg/m^3	Volume, %	Surface Area, cm^2/g	k_{25}, mol/m^2 s	E_a, kJ/mol
Quartz	SiO_2	2650	71.28	2.69E+01	1.26E-14	87.5
Glauconite	$K_{1.5}Mg_{0.5}Fe_{2.5}Fe_{0.5}AlSi_{7.5}O_{20}(OH)_4$	2750	4.4	1.60E+01	1.00E-14	58.62
Illite	$K_{0.6}Mg_{0.25}Al_{1.8}(Al_{0.5}Si_{3.5}O_{10})(OH)_2$	2750	2.64	9.60E+02	1.00E-14	58.62
Organic	CH_2O	1000	2.64	2.64E+00	1.00E-13	0
Kaolinite	$Al_2Si_2O_5(OH)_4$	2590	1.76	6.88E-01	1.00E-13	62.76
K-Feldspar	$KAlSi_3O8$	2560	1.76	6.80E+02	1.00E-12	67.83
Calcite	$CaCO_3$	2710	0.88	3.25E-01	1.60E-09	41.87
Dolomite	$CaMg(CO_3)_2$	2860	0.88	3.08E-01	6.00E-10	41.87
Oligoclase	$CaNa_4Al_6Si_{14}O_{40}$	2760	0.88	3.19E-01	1.00E-12	67.83
Siderite	$FeCO_3$	3940	0.88	2.23E-01	6.00E-10	41.87
Albite-low	$NaAlSi_3O_8$	2620	0	9.54E-01	1.00E-12	67.83
Alunite	$KAl_3(OH)_6(SO_4)_2$	1410	0	6.88E-01	6.50E-04	14.3
Anhydrite	$CaSO_4$	2960	0	6.88E-01	6.50E-04	14.3
Pyrite	FeS_2	5010	0	1.00E+01	2.82E-15	57.9
Smectite-Ca	$Ca_{0.145}Mg_{0.26}Al_{1.77}Si_{3.97}O_{10}(OH)_2$	2220	0	1.14E+02	1.00E-14	58.62
Smectite-Na	$Na_{0.29}Mg_{0.26}Al_{1.77}Si_{3.97}O_{10}(OH)_2$	2500	0	1.00E+02	1.00E-14	58.62
Goethite	FeOOH	4270	0	1.14E+02	1.00E-14	58.62

Results

Basalt

Supercritical CO_2 is sequestered rapidly in the basalt, precipitating in less than ten years (Figure 1). CO_2 is sequestered mainly as calcite, but also as dolomite and siderite with lesser amounts of dawsonite (Figure 2). All of the co-injected SO_2 is sequestered within 200 years (Figure 3), first as anhydrite and subsequently as pyrite (Figure 4). For the case considering co-sequestration of SO_2 at 1 km depth, pyrite precipitates more slowly. Extended simulations show that, after 1000 years, all the magnetite in the formation is consumed, removing a source of iron in solution, which causes pyrite to dissolve. After 5000 years, 86% of the pyrite remains at 1 km, 67% at 2 km, and 47% at 3 km.

The impact on basalt porosity resulting from co-injection of SO_2 with CO_2 is not significant for these simulations. Without CO_2 injection, over 5000 years porosity increases from 10% to 11.2% at 1 km depth, to 11.7% at 2 km depth, and to 12.4% at 3 km depth, mainly due to dissolution of magnetite and mesostasis. For the cases with either CO_2 injection alone, or co-injection of SO_2, over 5000 years porosity increases from 10% to 11.1% at 1 km depth, to 11.4% at 2 km depth, and to 12.2% at 3 km depth. Injection of CO_2/SO_2 initially causes a slight decrease in porosity, moderating the overall increase over time. Co-injection of SO_2 does not impact basalt porosity significantly versus CO_2 injection alone.

Dolomite

The dolomite formation is not favorable to mineral sequestration of CO_2, and actually dissolves slightly upon injection of supercritical CO_2 (Figure 5) due to dissolution of calcite. Dissolution of calcite does not appear to be enhanced by the addition of 1% SO_2. However, the calcium released into solution does facilitate the rapid precipitation of SO_2 as anhydrite (Figure 6) in less than two years. Extended simulations indicate that for this formation, the SO_2 will remain sequestered as anhydrite for at least 5000 years.

The impact on porosity resulting from co-injection of SO_2 with CO_2 is very slight. Without CO_2 injection, porosity does not change with time. With CO_2 injection, over 5000 years porosity increases by only 0.001%, because the dolomite formation does not sequester CO_2. For the cases with SO_2 co-injection, the porosity decreases by 0.003%, not a measureable change under real conditions.

Glauconitic Sandstone

The glauconitic sandstone is favorable to the mineral sequestration of supercritical CO_2 at depths of 2 km and 3 km, but sequestration rates are slow, and at 1 km depth a small amount of CO_2 is released (Figure 7). Even at 3 km depth only 20% of CO_2 is sequestered after 5000 years. Mineral sequestration of CO_2 occurs mainly via precipitation of dolomite, with lesser amounts of siderite. Mineral sequestration of SO_2 occurs via the precipitation of alunite, and is most favorable for long-term sequestration at 1 km (Figure 8). At this depth, 87% of the co-injected SO_2 has precipitated after 2000 years. At 2 km, alunite precipitation, and unfortunately, redissolution occurs more rapidly. Sixty percent of the injected SO_2 has precipitated as alunite after 500 years, but by 2000 years, only 15% remains sequestered. At 3 km, sequestration of injected SO_2 occurs only briefly. In this formation, alunite equilibrium is controlled mainly by the aqueous concentration of aluminum and pH; higher aluminum concentrations and pH drive alunite precipitation. As time goes on, kaolinite and K-feldspar precipitate, taking aluminum out of solution, and driving the dissolution of alunite. Anhydrite and pyrite do not precipitate; concentrations of calcium and iron in solution which would drive these reactions are suppressed by the precipitation of dolomite, siderite and goethite.

The impact on glauconite sandstone porosity resulting from co-injection of SO_2 with CO_2 increases with depth. Without CO_2 injection, the porosity remains constant at 12% at 1 km and 2 km depths, and decreases to 11% 3 km depth due to dissolution of quartz. With CO_2 injection, over 5000 years porosity remains constant at 12% at 1 km depth, decreases to 11.8% at 2 km depth, and to 10.9% at 3 km depth. There is no significant difference between the cases with and without co-injection of SO_2.

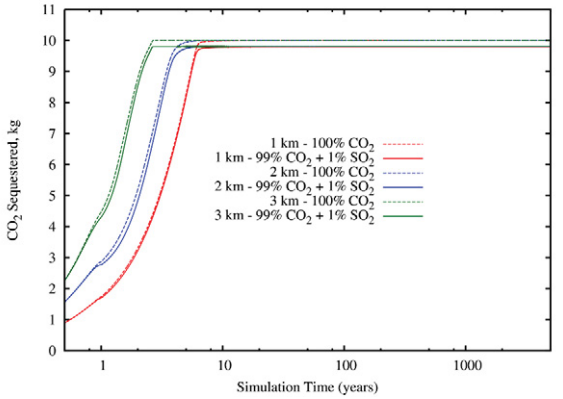

Figure 1. Comparison of mineral sequestration of CO_2 in basalt when injected alone or with 1% SO_2.

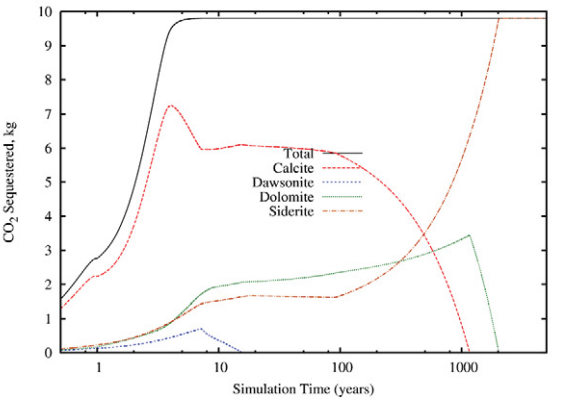

Figure 2. Carbonate minerals accounting for mineral sequestration of CO_2 in basalt when co-injected with 1% SO_2 at 2 km depth.

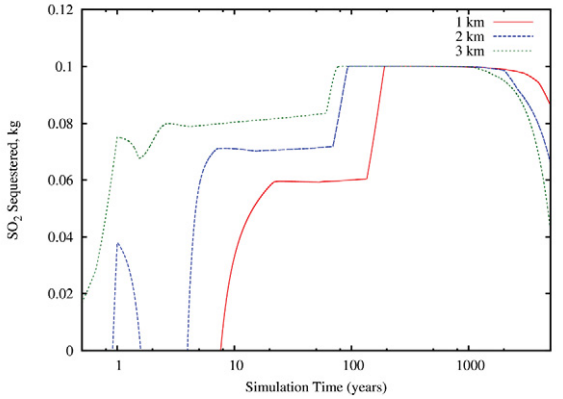

Figure 3. Comparison of mineral sequestration of SO_2 in basalt when co-injected with CO_2.

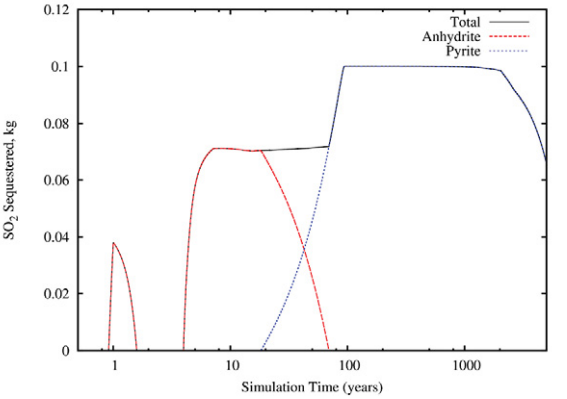

Figure 4. Comparison of mineral sequestration of SO_2 in basalt when co-injected with CO_2.

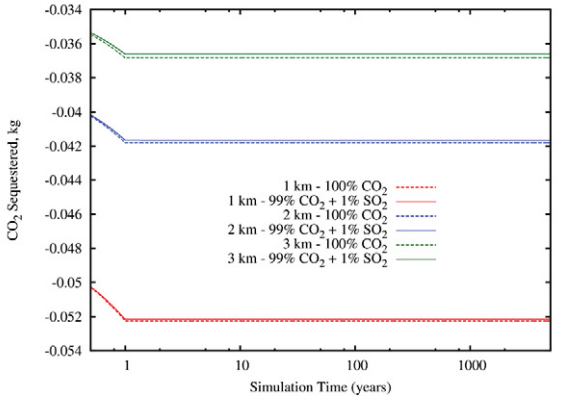

Figure 5. Comparison of mineral sequestration of CO_2 in dolomite when injected alone or with 1% SO_2.

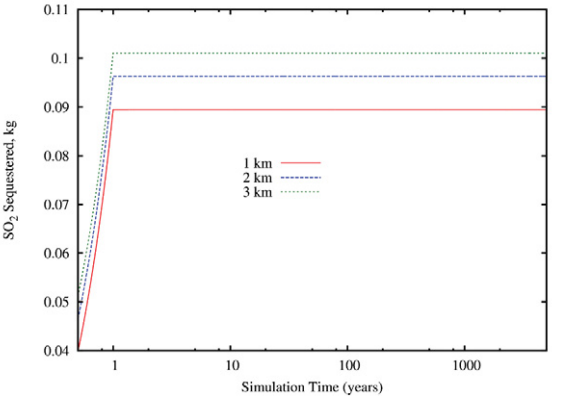

Figure 6. Comparison of mineral sequestration of SO_2 as anhydrite when co-injected with CO_2 into dolomite.

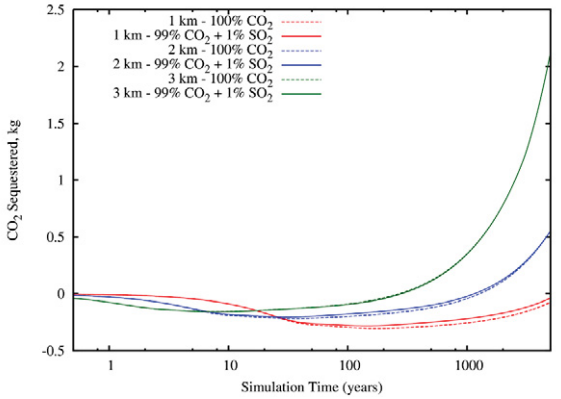

Figure 7. Comparison of mineral sequestration of CO_2 in glauconitic sandstone when injected alone or with 1% SO_2.

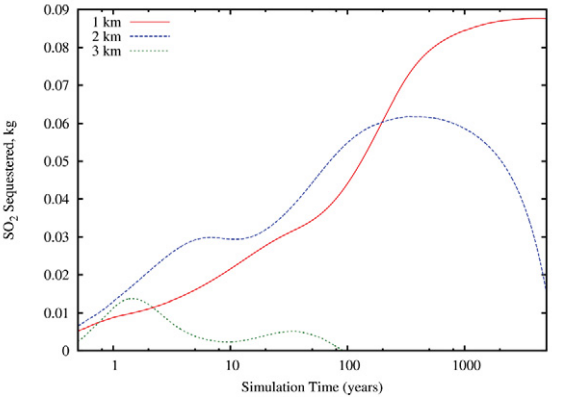

Figure 8. Comparison of mineral sequestration of SO_2 as alunite when co-injected with CO_2 into glauconitic sandstone.

Discussion

In considering whether co-sequestration is feasible in selected formations, several questions must be considered. First, does co-injection SO_2 significantly decrease the amount of mineral sequestration of CO_2? Second, how rapidly does sequestration of SO_2 occur? Third, is the co-injected SO_2 likely to be permanently sequestered in a mineral phase? Finally, does co-injection of SO_2 significantly impact formation porosity versus injection of CO_2 alone?

Co-injection of SO_2 lowers the pH of the formation water relative to injecting CO_2 alone. Co-injection of 1% SO_2 does not significantly reduce the sequestration of CO_2 in any of the three formations considered in this paper.

The rate of mineral sequestration of SO_2 increases with depth, due to higher mineral reaction rates at higher temperatures. Precipitation of anhydrite is rapid in both the dolomite and the basalt, but is eventually replaced by pyrite in the basalt. The rate of sequestration of SO_2 as alunite increases with depth in the glauconitic sandstone.

SO_2 sequestered as anhydrite in dolomite formations is predicted to be stable over long time periods, up to 5000 years. In basalt and in glauconitic sandstone, the amount of time SO_2 remains sequestered decreases with increasing depth, because the release rate of SO_2 caused by dissolution of the sequestering mineral increases with increasing depth. In the basalt, after 5000 years, 86% of SO_2 remains sequestered as pyrite at 1 km, versus 67% at 2 km and 47% at 3 km. In the glauconitic sandstone, after 5000 years, 87% of SO_2 remains sequestered as alunite at 1 km, versus 15% at 2 km and 0% at 3 km.

In all three formations, co-injection of 1% SO_2 did not induce a measureable change in porosity versus injection of CO_2 alone.

Acknowledgements

Funding for this work was provided under Pacific Northwest National Laboratory's Laboratory Directed Research and Development program. Prior development of carbon sequestration simulations in the basalt was funded by the Big Sky Carbon Sequestration Partnership under the Phase II Basalt Pilot Study. Prior development of carbon sequestration simulations in the dolomite was funded as part of the Ohio River Valley CO_2 Storage Project (sponsored by the U.S. Department of Energy, AEP, BP, Ohio Coal Development Office, Schlumberger, and Battelle along with its Pacific Northwest Division). Prior development of SO_2 co-sequestration simulations in dolomite were funded by Babcock and Wilcox.

References

1. White, M.D. and M. Oostrom, *STOMP: Subsurface Transport Over Multiple Phases, Version 4.0, User's Guide*. 2006, Pacific Northwest National Laboratory: Richland, Washington, PNNL-15782. p. 120.

2. White, M.D. and B.P. McGrail, *STOMP, Subsurface Transport Over Multiple Phases, Version 1.0, Addendum: ECKEChem, Equilibrium-Conservation-Kinetic Equation Chemistry and Reactive Transport*. 2005, Pacific Northwest National Laboratory: Richland, Washington, PNNL-15482.
3. Helgeson, H.C., *Thermodynamics of hydrothermal systems at elevated temperatures and pressures.* American Journal of Science, 1969. **267**(7): p. 729-&.
4. Xu, T., J.A. Apps, K. Pruess, and H. Yamamoto, *Numerical modeling of injection and mineral trapping of CO_2 with H_2S and SO_2 in a sandstone formation.* 2007.
5. Schaef, H.T., B.P. McGrail, and A.T. Owen, *Carbonate mineralization of volcanic province basalts.* International Journal of Greenhouse Gas Control, 2010. **4**(2): p. 249-261.
6. Wolery, T.W. and R.L. Jarek, *Software User's Manual, EQ3/6, Version 8.0*. 2003, Sandia National Laboratories: Albuquerque, New Mexico.
7. Palandri, J.L. and Y.K. Kharaka, *A Compilation of Rate Parameters of Water-Mineral Interaction Kinetics for Application to Geochemical Modeling*. 2004, U.S. Geological Survey: Menlo Park, California.
8. Xu, T.F., J.A. Apps, and K. Pruess, *Mineral sequestration of carbon dioxide in a sandstone-shale system.* Chemical Geology, 2005. **217**: p. 295-318.
9. McGrail, B.P., E.C. Sullivan, P.D. Thorne, F.A. Spane, Jr., C.J. Thompson, D.H. Bacon, S.P. Reidel, G. Hund, and F.S. Colwell, *Preliminary Hydrogeologic Characterization Results from the Wallula Basalt Pilot Study*. 2009, Battelle, Pacific Northwest Division: Richland, Washington, PNWD-4129.
10. Bacon, D.H., B.M. Sass, M. Bhargava, J. Sminchak, and N. Gupta, *Reactive Transport Modeling of CO_2 and SO_2 Injection into Deep Saline Formations and Their Effect on the Hydraulic Properties of Host Rocks.* Energy Procedia, 2009. **1**(3283-3290).
11. Bacon, D.H., M.D. White, N. Gupta, J.R. Sminchak, and M.E. Kelley, *CO_2 Injection Potential in the Rose Run Formation at the Mountaineer Power Plant, New Haven, West Virginia*, in *AAPG Studies in Geology # 59: Carbon Dioxide Sequestration in Geological Media - State of the Science*, M. Grobe, J.C. Pashin, and R.L. Dodge, Editors. 2009, American Association of Petroleum Geologists: Tulsa, Oklahoma.
12. Xu, T., J.A. Apps, and K. Pruess, *Analysis of Mineral Trapping for CO_2 Disposal in Deep Aquifers*. 2001, Lawrence Berkeley National Laboratory: Berkeley, California, LBNL-46992. p. 62.